UNCECOMP 2015
1st ECCOMAS Thematic Conference on
Uncertainty Quantification in Computational Sciences and Engineering
M. Papadrakakis, V. Papadopoulos, G. Stefanou (eds.)
Crete Island, Greece, 25–27 May 2015

UNCERTAINTY QUANTIFICATION AND MODELLING OF CFD SIMULATIONS OF A SWIRLING TURBULENT JET CREATED BY A ROTATING PIPE FOR APPLICATION TO HEAT TRANSFER FROM A HEATED SOLID FLAT PLATE

Francisco J. Granados-Ortiz[1], Joaquin Ortega-Casanova[2], and Choi-Hong Lai[3]

[1]Mathematical Sciences Department, University of Greenwich, London, UK
e-mail: gf13@gre.ac.uk

[2] Fluid Mechanics Department, University of Malaga, Malaga, Spain
e-mail: jortega@uma.es

[3] Mathematical Sciences Department, University of Greenwich, London, UK
e-mail: lc1@gre.ac.uk

Keywords: Uncertainty Quantification, Stochastic Collocation, Heat Transfer, Swirling Turbulent Jets, Impinging Swirling Jet, CFD modelling.

Abstract. *Swirling turbulent flows created by the rotation of pipes and applications for heat transfer can have interesting industrial purposes. As such physical phenomenon is under some physical uncertainties, it is interesting to understand their impact on the relevant parameters. In the present paper, the Stochastic Collocation method with Sparse Grids is developed, in order to study how the uncertainties are propagated from the Computational Fluid Dynamics (CFD) simulations of a Swirling jet created by the rotation of a pipe to the CFD simulations of the heat transfer from a flat plate by the impingement of the generated swirling jet. In addition, some mathematical models for the velocity profile and turbulent parameters are given, and their uncertainties studied, in order to facilitate this two-step process for industrial applications.*

1 Introduction

Swirling flows in pipes are widely used in industry, such as in erosion damage reduction [1] or dehydration systems in multi-phase flows [2]. The use of CFD softwares to model the behaviour of swirling flows is nowadays possible and it has become a deterministic way to simulate the physics of complex flows. The application of impinging jets to heat transfer purposes is also a very well-known mechanism to achieve an appropriate cooling in electronic components [3] & [4], surface varied plates [5] or impinging gases and flame jets [6] & [7], among others.
In the case under study, the impinging swirling jet is generated by a rotating pipe long enough to have a fully developed turbulent rotating flow at the end. For the heat transfer purpose, once the jet exits the pipe, it spreads in a bigger domain until it impinges against a heated at plate located at a dimensionless distance H/D from the exit pipe, where H represents the separation between the jet and the plate, and D is the diameter of the jet (diameter of the pipe, in fact). The Reynolds number is set to 23000 and the Swirl number to 1.
Uncertainties in volume-flow rate ($Q = 0.000361273$ m^3/s) and angular velocity of the pipe ($\Omega = 115$ rad/s) in the impinging swirling jet generation process, are translated into uncertainties in the exit of the pipe and heat transfer, which is quantified by the Nusselt number. In the present study, the uncertainty of the results is quantified by using Stochastic Collocation with Sparse Grids [8], and comparative results between the inclusion of mathematical models for the profiles computed by an User-Defined Function and its two-step CFD simulations for the heat transfer application are also presented.

2 Setting-Up the CFD Simulations

2.1 CFD Simulations of a Fully-Developed Turbulent Flow in a Rotating Pipe

Prior the simulation of the heat transfer, the impinging swirling jet is to be produced in a separated simulation of a rotating pipe. In Fig. 1, the pipe problem is depictured, for which a 2D RANS simulation was developed in Fluent. The flow under study goes out of the duct fully-developed, what requires to have a length bigger than a specific characteristic one. In order to avoid such as expensive analysis, a piece of pipe has been simulated with periodic boundary conditions, where a mass-flow rate is imposed according to the desired Reynolds number ($Re = \frac{4\rho Q}{\pi D \mu} = 23000$) and under rotating conditions set by the Swirl number ($S = \frac{\pi D^2 \Omega R}{4Q} = 1$), where ρ is the density of the fluid, Q is the volume-flow rate, μ is the dynamic viscosity and R is the radius of the pipe.

One of the biggest issues that a scientist can have simulating a flow is the choice of the turbulence model. The $k-\omega$ model has been widely used in CFD RANS simulations with very good agreement with experimental results in many CFD problems and there is a vast literature review with practical applications. But under some circumstances, a popular turbulence model like this one can not be the best one to simulate the physical behaviour of fluids. The simulation of a swirling flow is a particular application where turbulence models can fail. To solve the azimutal velocity can be problematic and this kind of flow has been studied in detail experimentally and computationally in several papers, such as [9] and [10].

To overcome this problem, more than 40 possible turbulent model configurations were tested to simulate the swirling flow confined in the rotating pipe with the computational mesh shown in Fig. 2. The size of the computational grid is $[n_r \times n_z] = 68 \times 450$ cells, obtaining a $y^+ < 1$

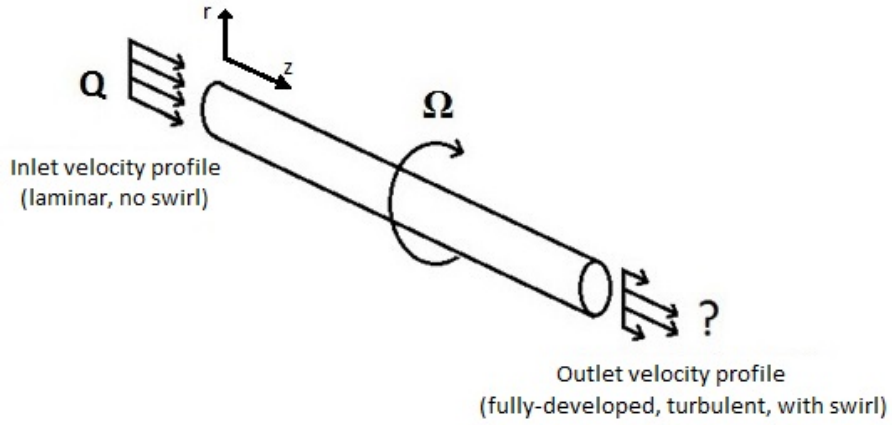

Figure 1: Sketch of the swirling flow generator by a rotating pipe.

along the walls of the pipe, and the discretization error (Grid Convergence Index, GCI) of the friction factor, λ , has been calculated following [18], having a discretization error of a 0.2% with 200 iterations per minute.

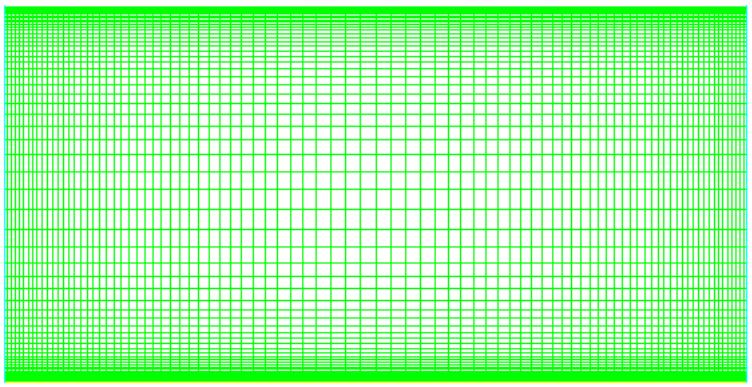

Figure 2: Computational grid for the pipe.

For the tested turbulence models, the best results took place with Reynolds Stress Model (RSM) Linear Pressure-Strain with Scalable, Standard Wall Functions, Enhanced Wall Treatment and Non-Equilibrium Wall Functions, RSM Quadratic Pressure-Strain with Scalable, Standard Wall Functions and Non-Equilibrium Wall Functions, $k-\epsilon$ Realizable with Enhanced Wall Treatment, SST $k-\omega$ and Standard $k-\omega$, as can be seen in Fig. 3, where both axial and azimutal dimensionless velocity profiles are represented and validated with the experimental results of Imao et al [9]. The chosen turbulence model was the Reynold Stress Model with Linear Pressure Strain and Enhanced Wall Treatment, as it is which better fits with these experiments.

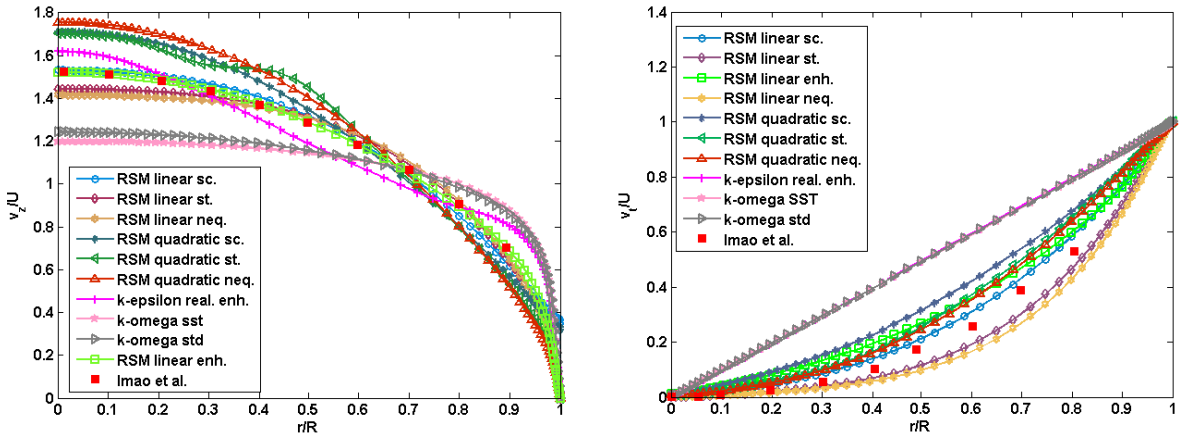

Figure 3: Plot of the axial and azimutal velocity profiles of the fully-developed turbulent swirling flow for several turbulence models and validation with Imao et al. $Re = 20000$ and $S = 1$.

2.2 CFD Simulations of the Heat Transfer from a Heated Solid Flat Plate from an Impinging Swirling Jet

Impinging jets for heat transfer have an extensive number of applications, as explained in section 1. The efficacy of the heat transfer will depend on different factors, such as the H/D distance, configuration of the jet or the surface of the plate [5]. Here, we are going to rely only on the configuration of the jet by controlling the angular velocity of the duct and the volume-flow rate as explained in section 2.1. In Fig. 4 a detail of the geometry and boundary conditions is depicted. The plate under consideration is totally flat (no roughness) and the distance between the exit of the duct and the plate is constant at $H/D = 5$, that represents the optimal distance to have the maximum global heat transfer, for a Re and S of the order under study.

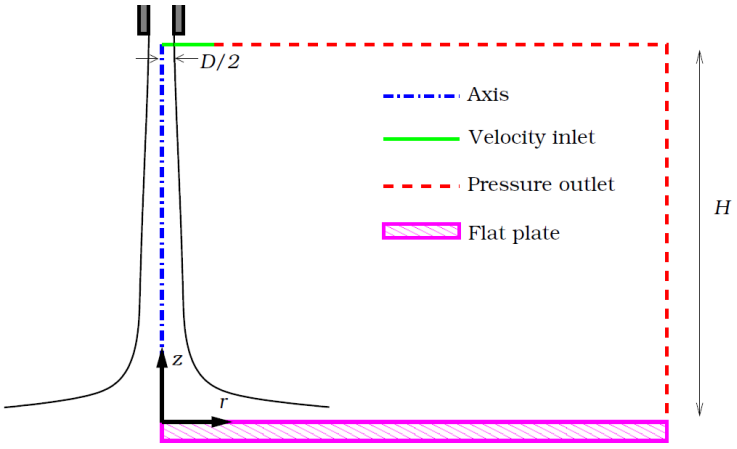

Figure 4: Sketch of the geometry and boundary conditions of the CFD simulations of the impinging jet.

The chosen turbulence model was the SST $k - \omega$ one, which provides a heat transfer result that fits very well with the experiments of [11] and [12]. A full description of this choice and the mesh can be found in [5].

2.3 Coupling the Two-Step CFD Simulations

As the turbulence model used for the duct and the one used for the impinging heat transfer problem are both different, a single simulation of the two-case scenario is not developed. Moreover, the complexity of the problem would be unnecessarily increased as the duct may be long enough to guarantee the fully-developed flow, so a huge domain should be simulated.
To overcome this problem, the two-step CFD simulations were coupled in the following way: firstly, the CFD simulations of the swirling flow confined in a rotating pipe with the RSM turbulent model were developed, and secondly, the velocity and $k-\omega$ dimensionless profiles at the exit of the pipe are used as inlet boundary conditions for the heat transfer simulation. The turbulent parameters are defined by (1) and (2:

$$k = \frac{2}{3}(UI)^2 \tag{1}$$

$$\omega = \rho\frac{k}{\mu}(\frac{\mu_t}{\mu})^{-1}, \tag{2}$$

where k is the turbulent kinetic energy, I is the turbulent intensity, U is the average velocity of the flow, ρ is the density of the fluid, ω is the turbulent dissipation rate and μ_t/μ is defined as the turbulent viscosity ratio. The turbulent kinetic energy is available from the RSM turbulent simulations, but the turbulent dissipation rate does not, so it has to be evaluated.

3 Uncertainty Quantification Process

3.1 Stochastic Collocation Method

For the Uncertainty Quantification method (UQ), the input uncertainties have been modelled by Uniform Probabilistic Distributions, and the Stochastic Collocation Method (SCM) with a Clenshaw-Curtis (C-C) Sparse Grid [8] has been implemented. SCM was developed by Mathelin and Hussaini [13] to improve the high costs of the Polynomial Chaos method. For each collocation point, the CFD problem is solved deterministically, and the solution can be constructed by interpolation (4), where $u_i(\mathbf{x}, t)$ are the deterministic solutions and l_i are the Lagrange interpolation polynomials, and statistical moments can be obtained by applying quadrature rules. SCM represents a very efficient option for lower dimension problems in comparison with sampling techniques such as Monte-Carlo. For higher dimension problems, sampling techniques use to be more suitable.
In the present paper, the collocation points of the Sparse Grid have been determined according to the C-C quadrature nested rule [14].
Special attention must be paid in the Probabilistic Density Function of the random variable, $\xi \in \Xi$, as we have to perform a mathematical transformation from the physical random variable space to an artificial stochastic space, called α-domain or α-space (3), that will depend on how the PDFs are defined. This transformation is an important difference with respect to other UQ methods.

$$\alpha = \mathcal{S}_\xi(\xi) \tag{3}$$

$$u(\mathbf{x}, t, \alpha) \approx \sum_{i=1}^{N} u_i(\mathbf{x}, t)\, l_i(\alpha) \tag{4}$$

Regarding the sources of uncertainty, they have been based on a literature review and the mechanical characteristics of a similar rotating pipe installation at University of Malaga. Depending on the installation and method used to measure, one may have different uncertainties in the experiments, but the idea of this research is to understand the propagation of uncertainties and sensitivities in the presented problem, based on realistic uncertainties from literature in the case when uncertainties from experiments are not available. For that aim, have been taken under consideration papers as [15], where a 2.5% of variation as uniform distribution in the Swirl number and inlet velocity was applied, that is a 2.5% for Q; [17], where a 3% of variation as uniform inlet velocity was applied; or [16], where a maximum of a 1% error for the velocity has been found for the described measurement techniques. Also, in the Fluid Mechanics laboratory of University of Malaga, the error of the available rotating pipe was analysed by engineers and it was found a 0.5% of variation for the angular velocity.

In the present problem, the Reynolds number under study is $Re = 23000$, as studied in [5], and the Swirl number is $S = 1$. For this situation, where the inflow is laminar flow water, the mean values of our uncertain parameters are $\bar{Q} = 0.000361273$ m^3/s and $\bar{\Omega} = 115$ rad/s. Within that framework, and trying to be conservative with respect to the literature results, the source of uncertainties have been determined as the uniform distributions $Q = \text{Unif}\,(-0,05\bar{Q}, 0,05\bar{Q})$ and $\Omega = \text{Unif}\,(-0,005\bar{\Omega}, 0,005\bar{\Omega})$. The turbulent intensity has been discarded from the uncertainty analysis as the flow confined in the pipe is fully-developed and the uncertainties in the turbulent intensity will not vary the results of the output parameters under study.

4 Uncertainty Quantification Results of the Two-Step CFD Simulation.

4.1 Uncertainty Quantification of the Turbulent Swirling Jet

For the first case scenario, we focused only on the simulated pipe, not simulating the impinging jet, as explained in section 2.1. Proceeding this way, we can avoid to perform very costly simulations, apply different turbulence models easily and, hence, have more control on the accuracy of the data.

The uncertainties of the CFD input parameters, Q and Ω, have a particular influence on the output of the simulations. In section 3.1, the Stochastic Collocation method has been presented, and the results of the mean and variance for different levels of the Clenshaw-Curtis quadrature using Sparse Grids can be observed in Table 1 & 2.

Level	Points	$\lambda_{r/R=1}$	$I(\%)_{r/R=0.5}$	$(v_z/U)_{r/R=0.5}$	$(v_t/U)_{r/R=0.5}$
1	5	0.01373401	8.45783368	1.28350388	0.26677295
2	13	0.01373399	8.45774137	1.28350593	0.26676999
3	29	0.01373404	8.45773429	1.28350567	0.26676957
4	65	0.01373401	8.45773957	1.28350436	0.26676961

Table 1: Stochastic means of the friction factor, turbulent intensity, dimensionless axial and azimutal velocity at $r/R = 0.5$ (m/s), at the exit of the rotating pipe.

Level	Points	$\lambda_{r/R=1}$	$I(\%)_{r/R=0.5}$	$(v_z/U)_{r/R=0.5}$	$(v_t/U)_{r/R=0.5}$
1	5	0.22152010e-06	0.72630289e-03	0.75705236e-04	0.22938667e-03
2	13	0.22059469e-06	0.72520829e-03	0.75256672e-04	0.22639809e-03
3	29	0.22066632e-06	0.72553382e-03	0.75245877e-04	0.22636540e-03
4	65	0.22067550e-06	0.72554659e-03	0.75261365e-04	0.22636600e-03

Table 2: Stochastic variances of the friction factor, turbulent intensity, dimensionless axial and azimutal velocity at $r/R = 0.5$ (m/s), at the exit of the rotating pipe.

For the present case, the most important outputs from the CFD simulations of the rotating pipe are the dimensionless velocity profiles and the dimensionless profiles of the turbulent parameters at the exit, as those profiles are used as inputs (inlet boundary conditions) for the coupled CFD problems. In Fig. 5 and 6 the mean and standard deviation envelopes of those profiles are shown.

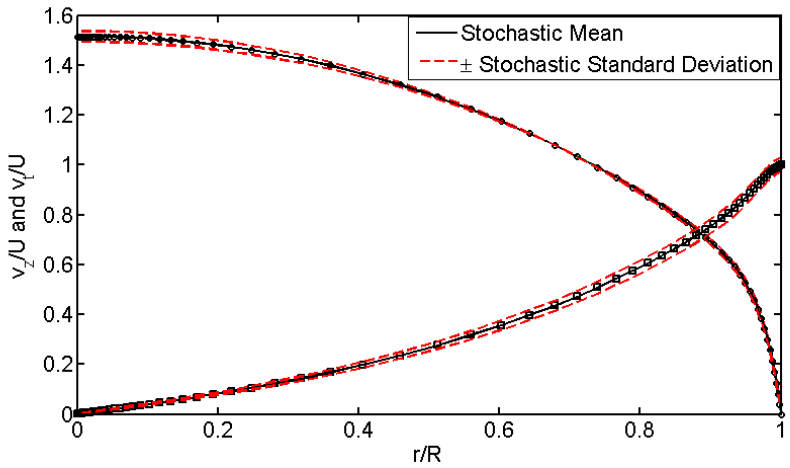

Figure 5: Radial distribution of the axial (○) and azimutal (□) dimensionless velocity profiles at the exit of the pipe for the level 4 of the C-C Sparse Grid.

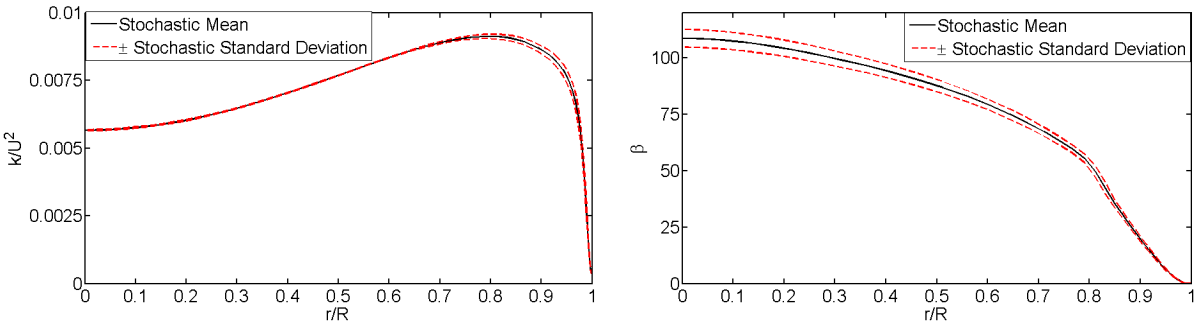

Figure 6: Radial distribution of the Turbulent Kinetic Energy, k, and the Turbulent Viscosity Ratio, β, at the exit of the pipe for the level 4 of the C-C Sparse Grid.

4.2 Uncertainty Quantification of the Impinging Swirling Jet applied to Heat Transfer from a Heated Solid Plate: Boundary Conditions from first-step CFD simulations.

For this second case scenario, we now focus on the heat transfer which takes place on the plate to an impinging jet generated in the previous step. To quantify the uncertainties in this problem, the Stochastic Collocation method with Clenshaw-Curtis Sparse Grid quadrature points are used again, in order to be consistent with the method and also use the deterministic simulations from the rotating pipe with relation to the Q and Ω uncertain parameters. For the deterministic simulations of the impinging jet domain, the correspondent velocity and turbulent profiles at the exit of the rotating pipe are used as inflow conditions. The simulations have been developed as 2D RANS in Fluent.

A detail of the meshed domain can be seen in Fig. 7. The size of the grid is $[n_x \times n_h]$ = 140×250 cells, with a $y^+ < 1$ along the plate. In practice, the x axis is the same as the r one when the pipe was analysed. Regarding the turbulence model, the SST $k - \omega$ has been chosen. This choice has been validated with the experimental data of impinging jets in [11] and [12], as can be also seen in Fig. 8. For further information about the computational features of the simulation, including the discretization error and the selection of the SST $k - \omega$ turbulence model, the authors suggest to see [5].

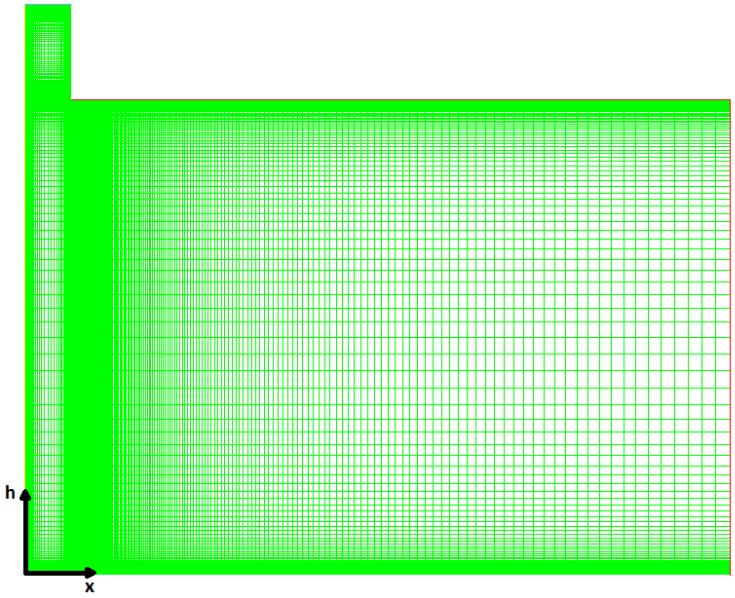

Figure 7: Computational grid for the CFD simulations of the impinging jet.

The uncertainties are propagated and they have an impact on the evolution of the Nusselt number along the plate. The mean and variance results for the SCM are presented in Tables 3 & 4. These results are for a dimensionless distance of $H/D = 5$.

The evolution of the Nusselt number along the plate, for $H/D = 5$, can be seen in Fig. 9, where it is represented with its standard deviation. It can be also observed that the most sensitive part to the input uncertainties is the peak that appears around $x/D = 0.33$, because of the evolu-

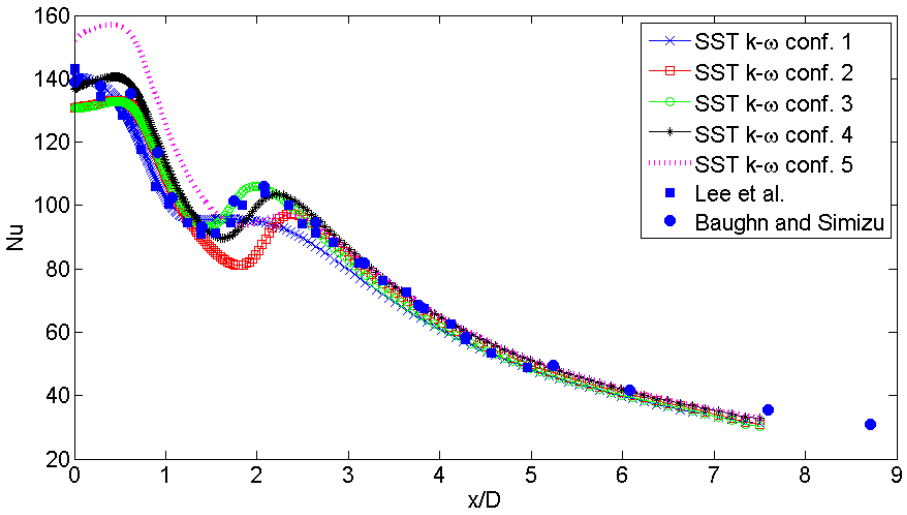

Figure 8: Validation of the turbulent model for $H/D = 2$. The different configurations of the SST $k-\omega$ turbulence model correspond to conf. 1: with transitional flow (old model in Fluent version 6.3), conf. 2: with Low Reynolds correction, conf. 3: without Low Reynolds correction, conf. 4: Transition SST with the Production Kato-Launder option and conf. 4: Transition SST with the Production Limiter option. The chosen option was SST $k-\omega$ with the Production Kato-Launder option.

Level	Points	Nu_0	Nu_{avg}
1	5	187.8183333	51.45473951
2	13	187.7914166	51.45413825
3	29	187.8031984	51.45457487
4	65	187.7993255	51.45497083

Table 3: Stochastic means of the Nusselt number at the stagnation point and its average value along the flat plate.

Level	Points	Nu_0	Nu_{avg}
1	5	15.24348189	1.50945541
2	13	15.56881637	1.50878302
3	29	15.47284719	1.50909036
4	65	15.47621431	1.50822473

Table 4: Stochastic variance of the Nusselt number at the stagnation point and its average value along the flat plate.

tion of the flow after impacting on the plate. This can be observed in the contour plots in Fig. 10.

4.3 Uncertainty Quantification of the Impinging Swirling Jet applied to Heat Transfer from a Heated Solid Plate: Use of a Model for the first-step CFD simulations.

For industrial purposes, as sometimes is expensive in terms of money and time to perfom CFD simulations or experiments, it is interesting to give models in order to avoid some parts of a complex analysis. In this paper, four dimensionless models are given: for the axial velocity, azimutal velocity, kinetic turbulent energy and turbulent viscosity ratio profiles, all of them for

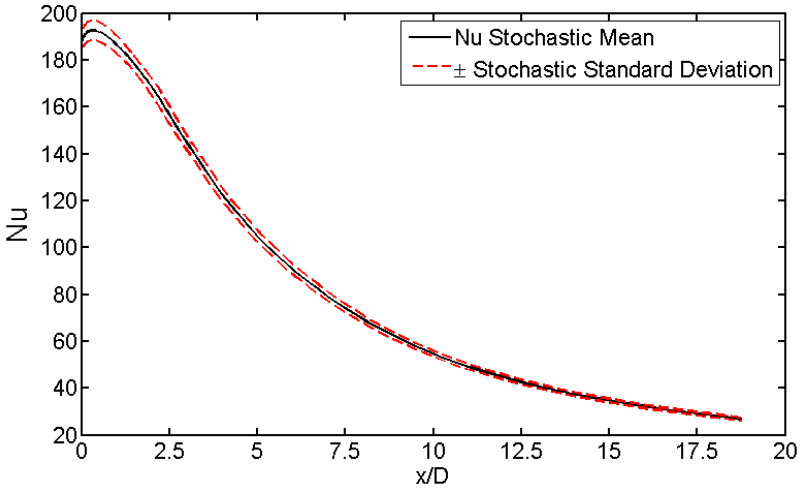

Figure 9: Evolution of the stochastic mean of the Nusselt number along the plate $\pm$ its stochastic standard deviation, for the $H/D = 5$ dimensionless distance and level 4 of the sparse grid.

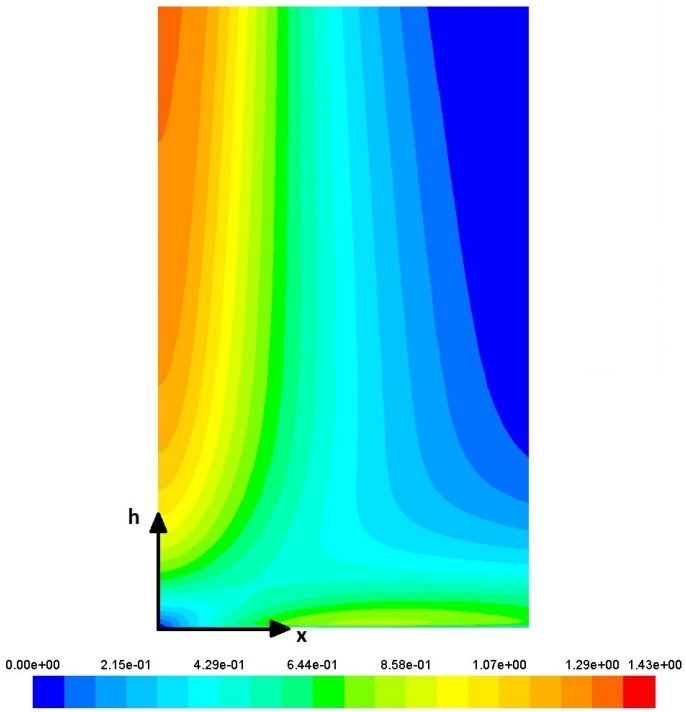

Figure 10: Detail of the contour plot of the dimensionless velocity nearby the coordinate of the peak in the evolution of the Nusselt number.

the fully-developed turbulent swirling flow case. Those models will approximate the response of the CFD RANS simulations for the different Q and Ω. This is what is often called *Meta-model*, *Surrogate Model* or *Surface Response Model*, and it represents a cheap way to assess computationally cost systems in some fields as, e. g., CFD optimisation or UQ, as it can be sampled with almost no computational cost. The mathematical models can be found in Eq. (5)-(8).

$$\frac{v_z}{U} = (a_z\,(\frac{r}{R})^3 + b_z\,e^{(-c_z\,\frac{r}{R}^2)})\,\frac{1}{2}\,(-\tanh(d_z\,\frac{r}{R} - 1)), \tag{5}$$

$$\frac{v_t}{U} = a_t\,(\frac{r}{R})^{b_t}, \tag{6}$$

$$\frac{k}{U^2} = (0.05327/(a_k + e^{b_k\,(\frac{r}{R})^{1.2}}\ \tanh(c_k\,(\frac{r}{R}) - 1), \tag{7}$$

$$\beta = a_\beta\,e^{-b_\beta\,(\frac{r}{R})^{c_\beta}}\,(e^{-d_\beta\,((\frac{r}{R})^{13}-1)} - 1), \tag{8}$$

These models are valid only in the intervals $Q \in [-0.05\bar{Q}, 0.05\bar{Q}]$ and $\Omega \in [-0.005\bar{\Omega}, 0.005\bar{\Omega}]$. The reason of do not use interpolation to construct the surrogate models is that more generic ones (valid for wider ranges) are under study by the authors, and in the present paper this models are shown just to give an indication of their usefulness. In addition, despite the goodness of the fitting models is really trustworthy, it is not presented here, as their description is extensive. To give an indication of the quality of the fit, Fig. 12 and 11 show the models for the non-perturbed input parameters.

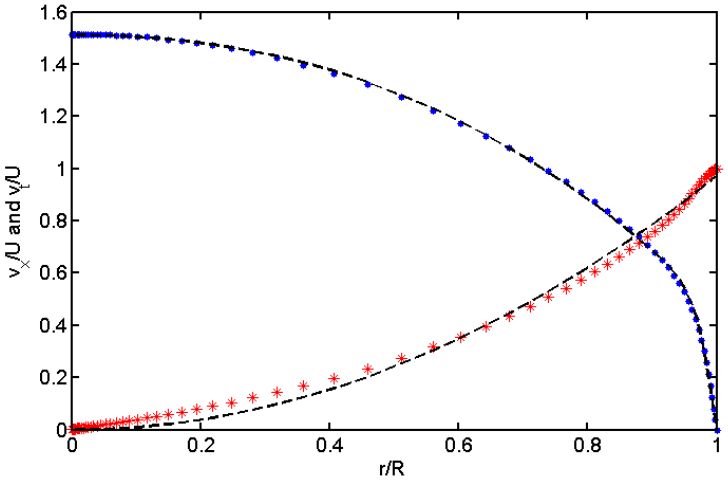

Figure 11: ($\bullet$) Axial velocity profile from CFD. ($*$) Azimutal velocity profile from CFD. (- -) Mathematical models.

The parameters α_i, where $\alpha = a, b, c, d$ and $i = z, t, k, \beta$, are constants of the fitting models, modelled by non-linear functions of Q and Ω, ready to be used as Boundary Conditions for new computational simulations.

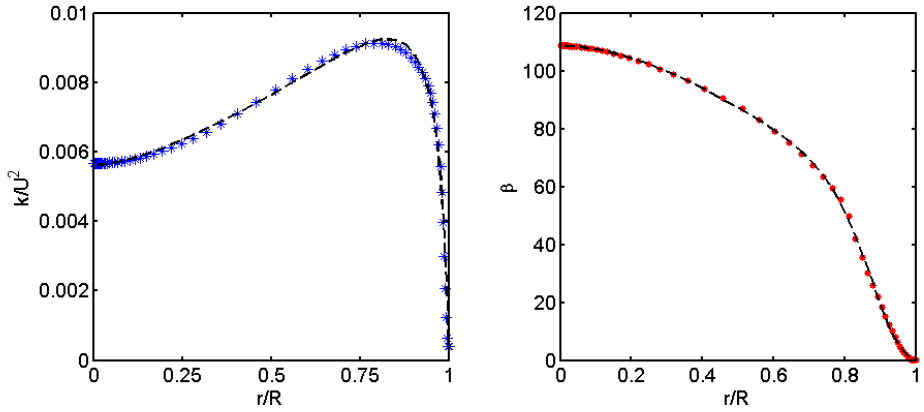

Figure 12: ($*$) Dimensionless k profile from CFD. ($\bullet$) Dimensionless β from CFD. (- -) Mathematical models.

To give an indication of the propagation of the errors when implementing the model by a User-Defined Function code in Fluent, the Stochastic Collocation method has been applied again for levels 1 and 2 of the Clenshaw-Curtis Sparse Grid, in order to compare with the CFD-based case. The results can be seen in Table 5 and 6. It can be seen that, despite the models fit very well with computational data, the small fitting errors are propagated through the simulation, having a relative error of almost an 8.7% between the variance of the Nusselt number at the stagnation point for the two analysed case scenarios. The other variations observed in the tables can be considered small.

Level	Points	Nu_0	Nu_{avg}	$Nu_{0,model}$	$Nu_{avg,model}$	$\epsilon_{r,Nu_0}(\%)$	$\epsilon_{r,Nu_{avg}}(\%)$
1	5	187.81833	51.454739	188.886500	51.245621	-0.5687	0.4064
2	13	187.79141	51.454138	188.859827	51.244494	-0.5689	0.4074

Table 5: Stochastic means of the Nusselt number case at the stagnation point and its average value along the flat plate. Relative error (in $\%$) between the CFD and model input results.

Level	Points	Nu_0	Nu_{avg}	$Nu_{0,model}$	$Nu_{avg,model}$	$\epsilon_{r,Nu_0}(\%)$	$\epsilon_{r,Nu_{avg}}(\%)$
1	5	15.243481	1.509455	16.467074	1.521298	-8.026989	-0.784601
2	13	15.568816	1.508783	16.930460	1.521590	-8.745970	-0.848853

Table 6: Stochastic variances of the Nusselt number case at the stagnation point and its average value along the flat plate. Relative error (in $\%$) between the CFD and model input results.

5 Conclusions

The Stochastic Collocation Method has been applied for uncertainty quantification to a two-step CFD simulation of a fully-developed turbulent swirling flow coupled to a second CFD simulation consisting on an impinging jet for heat transfer from a heated solid plate. The results showed that the physical uncertainties in Q and Ω slightly vary λ and the turbulent intensity.

In the dimensionless velocity profiles, it was noticed that the most sensitive part of the dimensionless axial velocity profile is $\frac{r}{R} = 0$, and $\frac{r}{R} = 1$ for the azimutal one. For the dimensionless Turbulent Kinetic Energy, $\frac{k}{U^2}$, the most sensitive area is the one located at the beginning of the decay, due to the strong effect of the wall. For the Turbulent Viscosity Ratio, β, the sensitivity is pretty similar to the dimensionless axial velocity one, having around the axis the biggest variances.
Regarding the heat transfer study, it has been observed that uncertainties in the input of the rotating pipe have a more notable impact in the Nusselt number along the plate than they had for the output parameters of the rotating pipe, particularly around $x/D = 0.33$, as a consequence of the physics of impingement and the selection of the turbulent model, as the peaks were different for different chosen models, as Fig. 8 shows.
Four models have been also given for the fully-developed state of the swirling flow confined in the rotating pipe, for the dimensionless profiles $\frac{v_z}{U}$, $\frac{v_t}{U}$, $\frac{k}{U^2}$ and β. These models fit very well with the computational ones, and a study of the propagated errors when implementing them in the uncertainty quantification has been given in section 4.3. This shows that the stagnation point is very sensitive to the fitting errors, as the increase of an 8.7% in the variance reveals.

6 Acknowledgements

The first author's professional development is supported by the FP7 AeroTraNet 2 Marie Curie Action. The first author also acknowledges Dr Jeroen A. S. Witteveen and Dr Paul Constantine for their suggestions in the beginning of this work.

REFERENCES

[1] Wood, R.J.K., Jones, T.F., Miles, N.J., and Ganeshalingam, J. Upstream swirl-induction for reduction of erosion damage from slurries in pipeline bends. *13th International Conference on Wear of Materials. Wear.* **250**, 112, 770-778, 2001.

[2] Hengwei, L., Zhongliang, L., Yongxun, F., Keyu, G., Tingmin, Y. Characteristics of a Supersonic Swirling Dehydration System of Natural Gas. *Chinese Journal of Chemical Engineering.* **13**, 1, 9-12, 2005.

[3] Hollworth, B.R., and Durbin, M. Impingement cooling of electronics.*Journal of Heat Transfer (Transactions of the ASME (American Society of Mechanical Engineers, Series C, USA)*, **114**, 3, 1992.

[4] Lee, D.H., Chung, Y.S., and Ligrani, P.M. Jet impingement cooling of chips equipped with multiple cylindrical pedestal. *Journal of Electronic Packaging*, **129**, 3, 221-228, 2007.

[5] Ortega-Casanova, J. and Granados-Ortiz, F. J. Numerical simulation of the heat transfer from a heated plate with surface variations to an impinging jet. *International Journal of Heat and Mass Transfer*, **76**, 128-143, 2014.

[6] Holger, M. Heat and Mass Transfer between Impinging Gas Jets and Solid Surfaces. *Advances in Heat Transfer*, **13**, 1-60, 1977.

[7] Viskanta, R. Heat transfer to impinging isothermal gas and flame jets. *Experimental Thermal and Fluid Science*, **6**, 2, 111-134, 1993.

[8] Smolyak, S.A. Quadrature and interpolation formulas for tensor products of certain classes of functions. *Soviet Math. Dokl.*, **4**, 240-243, 1963.

[9] Imao, S., Itoh, M., & Harada, T. Turbulent characteristics of the flow in an axially rotating pipe. *International journal of heat and fluid flow*, **17**, 5, 444-451, 1996.

[10] S. V. Poroseva. Wall corrections in modeling rotating flows. *Centre for Turbulence Research. Research Annuals*, 2001.

[11] Lee, D.H., Won, S.Y., Kim, Y.T., and Chung, Y.S. Turbulent heat transfer from a flat surface to a swirling round impinging jet. *International Journal of Heat and Mass Transfer*, **45**, 1, 223-227, 2002.

[12] Baughn, J.W., and Shimizu, S. Heat transfer measurements from a surface with uniform heat flux and an impinging jet. *Journal of Heat Transfer (Transactions of the ASME (American Society of Mechanical Engineers), Series C);(United States)*, **111**, 4, 1989.

[13] Mathelin, L. and Hussaini, M. Y., A Stochastic Collocation algorithm for uncertainty analysis, *Tech. Report NASA/CR-2003-212153, NASA Langley Research Center*, 2003.

[14] Von Winckel, G. Fast Clenshaw-Curtis quadrature. The Mathworks Central File Exchange, Mar. 2008. URL http://www.mathworks.com/matlabcentral/fileexchange/19063-sparse-grid-quadrature/content/spquad.m.

[15] Congedo, P. M., Duprat, C., Balarac, G., & Corre, C.. Effects of inlet uncertainties on prediction of turbulent flows using RANS and LES simulations. *20th AIAA Computational Fluid Dynamics Conference*, 2011.

[16] Bailey, S. C. C., Hultmark, M., Monty, J. P., Alfredsson, P. H., Chong, M. S., Duncan, R. D., & Vinuesa, R. Obtaining accurate mean velocity measurements in high Reynolds number turbulent boundary layers using Pitot tubes. *Journal of Fluid Mechanics*, **715**, 642-670, 2013.

[17] Brugiere, O., Balarac, G., Corre, C., Metais, O., & Flores, E. Numerical prediction of a draft tube flow taking into account uncertain inlet conditions. *IOP Conference Series: Earth and Environmental Science*, **15**, 3, 32-39, 2012.

[18] Celik, I.B., Ghia, U., and Roache, P.J. Procedure for estimation and reporting of uncertainty due to discretization in CFD applications. *Journal of Fluids Engineering-Transactions of the ASME*, **130**, 7, 2008.